



Establishing Equal-Channel Angular Pressing (ECAP) for sheet metals by using backpressure: manufacturing of high-strength aluminum AA5083 sheets

Maximilian Gruber¹ · Christian Illgen² · Felix Lichte¹ · Christoph Hartmann¹ · Philipp Frint^{2,3} · Martin F.-X. Wagner² · Wolfram Volk¹

Received: 16 February 2023 / Accepted: 30 May 2023 / Published online: 14 June 2023

© The Author(s) 2023

Abstract

Severe plastic deformation (SPD) processes offer the possibility of improving the mechanical properties of metallic materials by grain refinement. However, this great potential has so far mostly been applied on a laboratory scale or on small series. Equal-Channel Angular Pressing (ECAP) also enables to integrate the advantages in industrial processes with large output—so far, mainly for bars or thick plates. In this paper, we investigate the ECAP process for sheet metal. Preliminary investigations have shown that cracks form on the surface when aluminum AA5083 sheets are processed. To solve this problem, we determined the Johnson–Cook fracture criterion for the material and modeled the process numerically. The simulation was carried out with the superposition of a backpressure and subsequently implemented and validated experimentally. The semi-finished sheet metal products from the ECAP investigation were then mechanically characterized with microhardness measurements and tensile tests. In addition, the microstructure was investigated with Electron Back Scatter Diffraction (EBSD). Even comparatively small amounts of backpressure (10 MPa) already result in a significant suppression of the crack formation in the numerical and experimental investigations. The microhardness measurements indicate a more homogeneous strain distribution for a sufficient level of applied backpressure which enables the processing of crack-free sheets in multiple ECAP passes. As with ECAP of bulk materials, tensile tests on the processed sheets show a reduced elongation to failure (–73%) but a significantly increased yield strength (+157%) compared to the initial condition of the material. Distinct substructures are found in the EBSD measurements and explain this behavior. The findings provide the basis for using ECAP on an application-oriented scale and demonstrate an advanced manufacturing method for the production of high-strength aluminum sheets.

Keywords Equal-Channel Angular Pressing (ECAP) · Johnson–Cook fracture criterion · FEM simulation · Aluminum AA5083

1 Introduction

Due to the growing climate awareness in society and economy, a change in environmental strategy is increasingly expected from industrial companies. Particularly in the

transportation and mobility industry, companies are required by law to design products and processes that are more environmentally friendly and sustainable. To achieve this, many companies are using materials that reduce the weight of the final product. Intelligent lightweight construction can reduce the energy consumption and thus achieve a more CO₂-friendly result. In the choice of materials that can be used for this purpose, aluminum will come into even sharper focus by the year 2030 [1]. Despite the obvious advantages, it also has limitations in terms of cost and mechanical strength, which so far restrict its use, especially in the bodywork and crash structures of the automotive industry.

Severe plastic deformation (SPD) processes offer the possibility of increasing the strengths of metallic materials

✉ Maximilian Gruber
Maximilian.gruber@utg.de

¹ Chair of Metal Forming and Casting, Technical University of Munich, 85748 Garching, Germany

² Institute of Materials Science and Engineering, Chemnitz University of Technology, 09125 Chemnitz, Germany

³ Nordmetall GmbH, 09221 Neukirchen, Germany

and thus expanding the previously mentioned fields of application [2]. The process is based on the introduction of shear strains into the material, whereby substructures with low-angle as well as new high-angle grain boundaries can be formed if a sufficient amount of plastic deformation is applied [3]. The additional grain boundaries are effective obstacles for dislocation motion during further deformation, resulting in macroscopically increased strength [4]. However, these processes usually require a large effort in terms of time and energy. As a result, most of the development of existing processes takes place at the laboratory scale and is thus limited to small quantities [5]. Equal-Channel Angular Pressing (ECAP), in particular, is one of these processes that also addresses the possibility of use on an industrial scale [6]. In ECAP, material is pressed through an angled channel, introducing a large shear strain into the material. This results in severe plastic deformation of the microstructure without altering the macroscopic dimensions of the material [7]. Two major problems of the ECAP process are inhomogeneities occurring in the microstructure of the billet's cross-section [8, 9] as well as pronounced crack formation on the material's surface [10, 11] (see Fig. 1). To solve these issues, a superposition of pressure by a counterholder was originally proposed in the so-called Equal-Channel Angular Extrusion (ECAE) approach [12]. By superimposing compressive stresses, cracking and void formation on the surface could be suppressed. In addition, the material could be pressed into the outer radius of the angled die by the backpressure, resulting in a more sharply defined plastic deformation zone (PDZ) characterized by a smaller opening angle and a more uniform microstructure [13]. Figueiredo et al. used numerical studies with a Cockcroft-Latham fracture criterion to investigate process control with a backpressure of 80 MPa for magnesium deformed at different of strain rates [14]. Frint et al. used a backpressure of up to 200 MPa for the ECAP of aluminum 6060 to obtain a homogeneous and crack-free structure [15]. Stolyarov et al. performed ECAP on aluminum bars with a backpressure of 275 MPa and were able to reach 16 passes of ECAP, but with a reduction in strength compared to a backpressure of 100 MPa [16]. Another way to increase the strains and obtain a more homogeneous microstructure is multiple forming using

ECAP [17]. It is well documented that the route C (180° rotation around the ECAP direction for a second pass) contributes to the formation of a homogeneous microstructure [18].

All of these studies deal with the ECAP of bars or bulk material. Lightweight applications in the automotive industry, however, create a need for materials with other dimensions—such as sheet metals. In general, the ratio of surface area to volume for semi-finished sheet metal products increases in comparison to semi-finished products with a round or square cross-section. This causes the influence of friction on a larger area and defects on the surface have a significantly greater influence on the semi-finished product properties (see Fig. 1c). In addition, sheet cross-sections run the risk of buckling or wrinkling. The ECAP processes, which process aluminum alloys as semi-finished sheet products and generate high shear deformations in the process, exhibit these scalability issues and achieve lower mechanical properties compared to conventional ECAP.

In previous studies, we already performed investigations with an ECAP tool that is able to process aluminum sheets with a thickness of 1.8 mm and a size of 200 × 160 mm (length × width) (see Fig. 2a). To perform the ECAP test, the sheet is placed in the channel between the left and right channel parts and pressed with the stamp (speed = 6 mm/s) through the angle at the end of the channel. The tool parameters are shown in Fig. 2b. Using this tool, it was possible to promote the onset of microstructural changes in the sheets and to perform ECAP with different routes [19]. Numerical investigations within these first studies have already identified possibilities to improve the channel geometry with respect to further increased shear strains. Here, the influence of the inner channel radius and the channel angle were investigated in particular [20]. However, further experimental investigations showed that surface defects occur in ECAP for aluminum alloy AA5083 sheet materials with increasing strains (see Fig. 2c). For this experiment, the channel radius of the right channel part (inner radius) is $r = 0.3$ mm, and that of the left channel part is $R = 2.3$ mm. The active elements form a channel angle of $\Phi = 100^\circ$ and a width $w = 2.1$ and height $h = 2.1$ mm were chosen.

Fig. 1 Major problems for the processing of aluminum with ECAP: (a) inhomogeneities; (b) surface cracks; (c) scalability

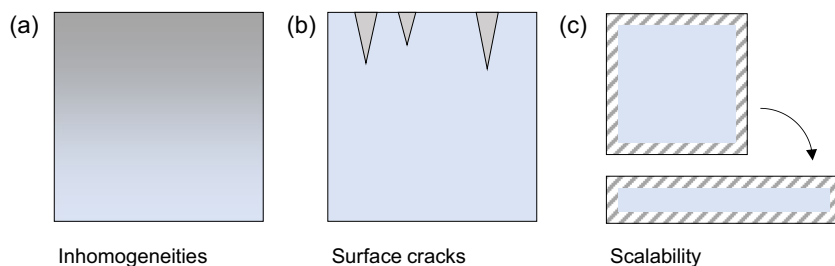
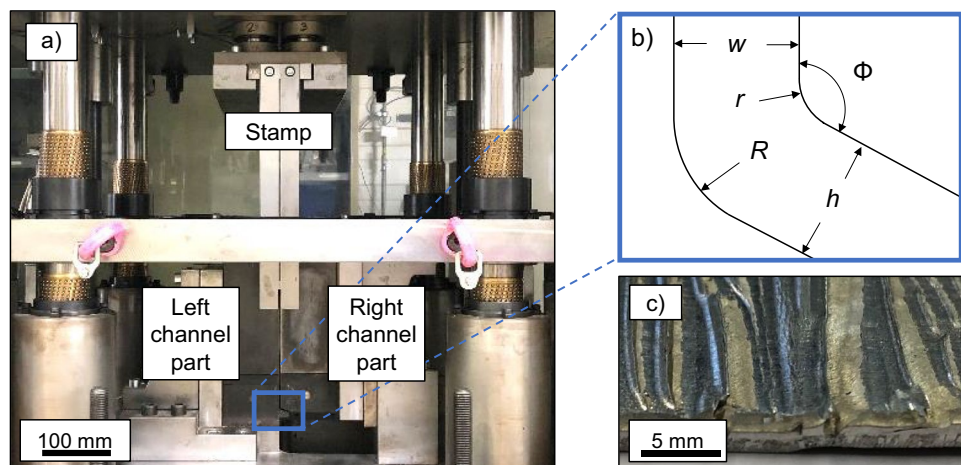


Fig. 2 (a) ECAP tool consisting of the left and right channel parts and the stamp; (b) schematic sketch of the ECAP channel with the geometrical parameters; (c) cracks occur on the sheet metal surface



In order to solve the two main problems of the ECAP process (inhomogeneities and cracks) also for ECAP of sheet materials, this study presents simulations based on a numerical finite element model (FEM). To address the problem of crack formation, a fracture model for sheet metal ECAP processes is developed. The simulation is then utilized to design the use of backpressure and thus to improve the resulting microstructures and sheet surfaces. Finally, the mechanical properties of the ECAP sheets are tested to evaluate the improvement of the material and the influence of the backpressure. This work provides a framework for future research and a blueprint for practical integration of the ECAP manufacturing technique into industrial processes that handle semi-finished sheet metal products.

2 Material and methods

2.1 Sheet material and mechanical testing

For the ECAP experiments in this study, we used cold-rolled aluminum AA5083 sheets (4.81 wt% Mg, 0.53 wt% Mn, 0.36 wt% Si, 0.23 wt% Fe, and 0.18 wt% Cr, bal. Al). The dimension of the sheet material was 200 mm × 160 mm with a sheet thickness of ~1.8 mm. The rolling direction (RD) is aligned along the longer side (200 mm). Prior to deformation in our ECAP tool, the sheets were subjected to a homogenization heat treatment for 1 h at 500 °C. This homogenized state is referred to in the following as the reference state (Ref).

To characterize the mechanical properties, tensile specimens (DIN 50125 shape E, width 10 mm, parallel length 45 mm) were machined from the initial material (Ref) and the ECAP sheets [21]. The specimens were tested quasi-statically in a Zwick ZT150 Allround Line universal testing machine according to [22]. A test speed of 0.0375 mm/s was selected with position-controlled

setting, which corresponds to a nominal strain rate of about 10^{-3} s^{-1} . Strains were measured using Digital Image Correlation (DIC) with a GOM Aramis SRX system. Moreover, hydraulic bulge tests according to DIN EN ISO 16808 were performed to select a suitable extrapolation for the flow curve [23]. In this study, the approaches according to Gosh and Hockett-Sherby were combined with a factor $\alpha = 0.265$, whereby the Gosh extrapolation accounts for the smaller portion. [24, 25]. Figure 3 shows the determined flow curve with this extrapolation and Table 1 summarizes the values used for the simulation. Three samples were taken for each tensile test with ECAP and Ref state each and also three tests for the bulge tests.

After ECAP, microhardness tests were performed to evaluate the homogeneity of the deformed microstructures. For this purpose, specimens were cut from the formed ECAP sheets parallel to the ECAP direction (ED). The samples were mechanically ground with SiC paper (800–2500 grit) and polished with an oxide polishing suspension of 0.05 μm . A Vickers indenter with a load of

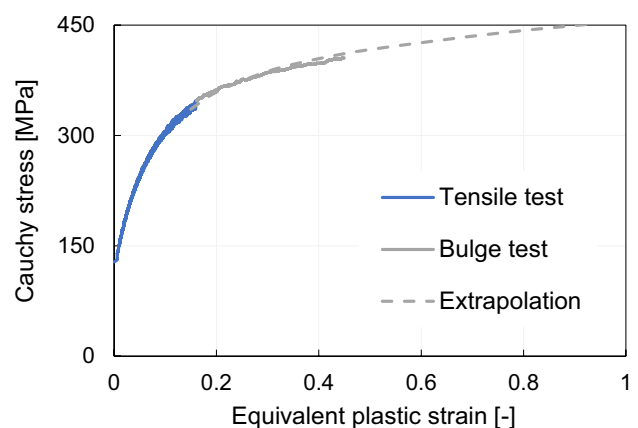


Fig. 3 Extrapolated flow curve of the aluminum alloy AA5083 determined from tensile and bulge test data

Table 1 Rounded equivalent plastic strain [-] and cauchy stress [MPa] values of the flow curve used for the numerical investigations

Equ. plastic strain [-]	0	0.006	0.008	0.01	0.02	0.03	0.05	0.07	0.1	0.2	0.5	1	1.5	2
Cauchy stress [MPa]	130.4	130.5	139	147	179	204	241	269	301	359	417	456	482	502

0.1 N was applied. The measuring points were started at the edge of the outer radius with a distance of 0.05 mm. Then, the measuring points were placed sideways (alternately left and right) with a distance of 0.3 mm (in ECAP direction) and with lateral offset of 0.15 mm over the sheet thickness to determine the microhardness values, see also [20]. To validate the statistics, three measurements were used on two different ECAP samples each and the mean values and standard deviations were calculated (six measured values per measuring point).

2.2 Material modeling for numerical analysis

ECAP for bulk material has already been intensively investigated in simulation studies. Strain hardening was for example investigated analytical and compared to numerical results [26], strain path dependence was analyzed [27] and in a current study strain homogeneity was investigated for round billets [28]. In the present paper, the simulations were done specifically for sheet metal, so sheet material was used for material characterization and modeling.

To address the problem of cracking in the numerical analysis of ECAP processing, the following section presents the investigation of the fracture behavior of the AA5083 material using the push-out test to determine the Johnson–Cook fracture criterion. This methodology was chosen to represent a similar condition as in the ECAP process. During the cutting process of the push-out test, a shear stress state is present across the sheet cross-section similar to ECAP. To ensure comparability of the stress states, the triaxialities of the two processes were compared in the simulations and discussed in the numerical results.

In our study, the determination of the necessary parameters was carried out by inverse parameter determination according to Greß et al. [29]. For this purpose, push-out experiments were performed and matched with simulations. The parameters of the Johnson–Cook model were iteratively adjusted in the simulation so that the failure behavior agrees numerically and experimentally. The Johnson–Cook fracture criterion is limited to a small number of constant parameters. Primarily, the model is based on the strain and strain rate as well as temperature and pressure [30]:

$$\bar{\varepsilon}_f = (D_1 + D_2 e^{D_3 \eta}) \left[1 + D_4 \ln \left(\frac{\dot{\varepsilon}}{\dot{\varepsilon}_0} \right) \right] (1 + D_5 \theta)$$

Here, $\bar{\varepsilon}_f$ describes the plastic strain at which fracture begins. The Johnson–Cook material constants are represented by the parameters D_1 to D_5 . D_1 , D_2 , and D_3 explain how the hydrostatic stress affects the fracture strain. D_4 describes the influence of strain rate and D_5 the influence of temperature on the fracture strain. e describes the equivalent plastic strain, η the stress triaxiality, $\dot{\varepsilon}_0$ the reference strain rate, $\dot{\varepsilon}$ the effective strain rate, and θ the temperature. As the ECAP experiment was performed at room temperature, this parameter was therefore neglected in this context. In addition, the material is not sensitive to strain rates at the low forming speeds, so this aspect is also neglected [31]. This step simplifies the equation to

$$\bar{\varepsilon}_f = (D_1 + D_2 e^{D_3 \eta})$$

The stress triaxiality η is composed of the ratio of the hydrostatic stress (p) to the Mises equivalent stress (q) and is dimensionless. It is calculated as follows, where σ_1 , σ_2 , and σ_3 represent the normal stresses:

$$\eta = \frac{p}{q}$$

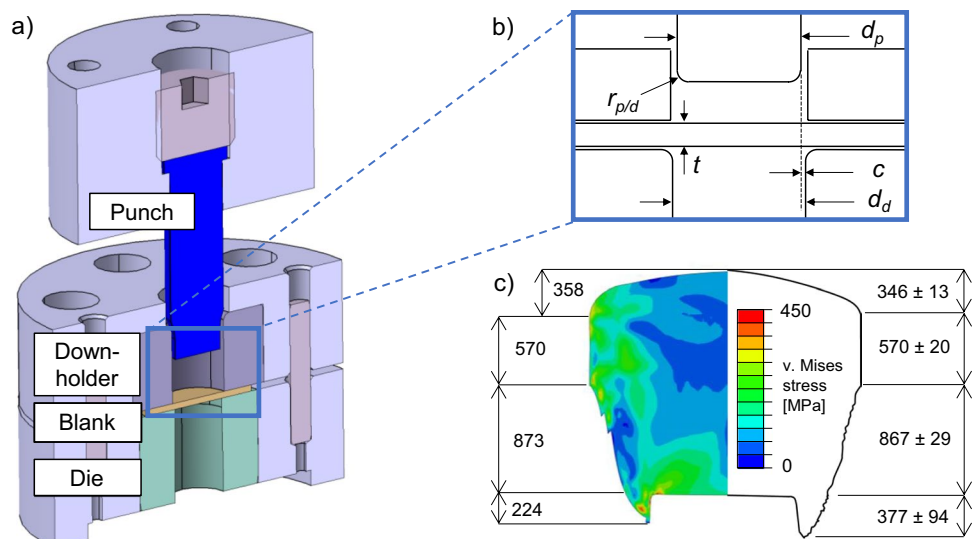
$$p = \frac{\sigma_1 + \sigma_2 + \sigma_3}{3}$$

$$q = \sqrt{\frac{1}{2} \left[(\sigma_1 - \sigma_2)^2 + (\sigma_3 - \sigma_2)^2 + (\sigma_1 - \sigma_3)^2 \right]}$$

For the determination of the material constants D_1 , D_2 , and D_3 , push-out tests were carried out (see Fig. 4). The die was mounted in a Zwick ZT150 Allround Line universal testing machine. The disk-shaped AA5083 specimen (thickness $t = 1.8$ mm) was clamped by the downholder onto the die (diameter $d_d = 18$ mm; $r_d = 0.06$ mm). The punch (diameter $d_p = 17$ mm; $r_p = 0.06$ mm; die gap $c = 0.5$ mm) was attached to the cross-head of the universal testing machine and moved with a constant speed of 1 mm/min until failure occurred in the aluminum specimen.

The shear zone was analyzed optically. For this purpose, the specimens were cut in half and the cross-section was ground and polished. With a digital microscope (Keyence VHX 2000), the exposed cutting surfaces were measured for their characteristics. It is important to note the differentiation of the individual cut areas according

Fig. 4 (a) CAD model of the push-out test; (b) schematic sketch of the push-out test with the geometrical parameters; (c) numerical (left) and experimental (right) results of the push-out test



to VDI guideline 2906–2: edge indentation, smooth cut, fracture surface, and burr [32]. Particularly for the examination of aluminum AA5083, a distinct and long burr can be observed (Fig. 4c), as already noted by Greß et al. [33].

Using the program Abaqus/Explicit Version 2020, the setup of the push-out test on aluminum AA5083 was simulated. The simulation was built up in a two-dimensional, axisymmetric model. For sufficient comparability, it is important to reproduce the exact dimensions and material properties of the test. The punch, die, and downholder were simulated as analytical rigid bodies. The material AA5083 was defined as a deformable solid. The previously determined flow curve and the material parameters from the numerical studies of [34] were used. In order to use the computational capacity efficiently and still allow for an accurate investigation of the cutting zone, a finer meshing of an element edge length of 0.025 mm inside the shear zone, as opposed to 0.25 mm outside the shear zone, was specified. In addition, a mass scaling with a target time increment of $5 \cdot 10^{-07}$ was used. “Hard contact,” stored in Abaqus, was used and the friction was modeled as isotropic penalty with a Coulomb friction of 0.1. The Johnson–Cook parameters D_1 , D_2 , and D_3 were inversely determined by matching and calibrating with experimental results using the method of Greß et al. [29]. The focus was placed on the smooth cut portion, which plays an important role for the onset of fracture. Less emphasis was placed on the formation of the burr, which is also subject to greater fluctuation in the experiment than the other parameters. Figure 2c shows the comparison of the numerical results and the experimentally determined cut surfaces. The experimental results (on the right side) are provided with the scatter values from three specimens. The contour of a single experimentally tested specimen

is shown (on the left side) as an example. The iteratively determined parameters are $D_1 = 0.1$; $D_2 = 7$; $D_3 = 16$.

3 Numerical investigations on sheet metal ECAP

As in the determination of the Johnson–Cook parameters, the explicit code Abaqus 2020 was used. The simulation is set up in 2D with a plane strain formulation. This assumption is made because the plate width of 160 mm is large compared to the plate thickness of 1.8 mm and, accordingly, there is a homogeneous strain state across the plate width. The channel and the stamp were modeled as analytical rigids (see Fig. 5a). The sheet was meshed with rhomboid-shaped elements (CPE4R). Different mesh sizes were tested in terms of result accuracy and computation time and an element edge length of 0.15 mm. Rounding the bottom edge of the

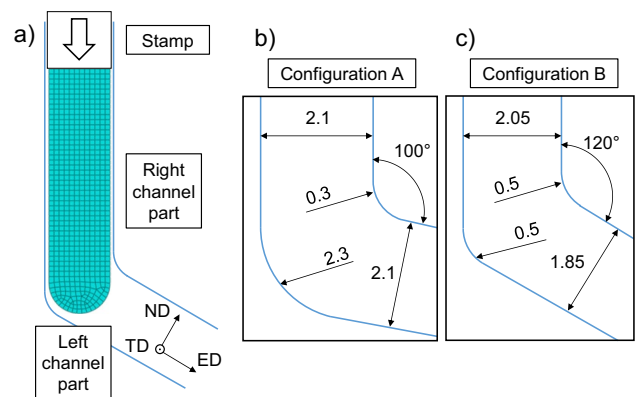


Fig. 5 (a) Schematic sketch of the simulation model; overview of the two geometrical setups used in this study: (b) configuration A; (c) configuration B

sheet helps to prevent numerical problems. For the contact, the “hard contact” stored in Abaqus was used, and the friction was modeled as isotropic penalty. A friction coefficient of 0.04 was used for the lubricated process, which corresponds to the determined values of previous studies [34]. For analyzing the ECAP process, two different parameter configurations were modeled: *configuration A* has the same geometrical parameters as in the experimental preliminary studies, where the cracks on the surface occurred: $w=2.1$ mm, $h=2.1$ mm, $\Phi=100^\circ$, $R=2.3$ mm, $r=0.3$ mm. In addition, *configuration B* was designed in order to test the influence and potential of a sharper outer radius: $w=2.05$ mm, $h=1.85$ mm, $\Phi=120^\circ$, $R=0.5$ mm, $r=0.5$ mm. Figure 5 gives an overview of the two geometries.

Different mass scalings were tested to obtain adequate computing times and a target time increment of $5 \cdot 10^{-5}$ was used because it offers a good compromise between result accuracy and computing time (see Fig. 6).

To ensure comparability of the stress states, the triaxialities of the two processes were compared in the simulation. For the push-out test, only elements close to the fracture zone were evaluated (9 elements). Implausible values were excluded (triaxiality < -2). For the ECAP sheet, all elements were selected and the triaxiality was averaged, excluding the upper and lower quartiles to disregard outliers. For

both processes, the value is about -1 and the assumption of comparability holds. The value does not correspond to pure shear, but to a superimposed compressive stress, which is related to the fact that during both processes the material is in contact with the tools and therefore experiences a pressure superposition.

By determining the Johnson–Cook parameters, it was also possible to reproduce the crack formation in the numerical investigations. In order to ensure a complete calculation of the simulation without aborting, the element deletion was turned off in the ECAP simulation. To investigate the cracking nevertheless, elements with a Mises stress of less than 0.01 MPa and greater than 500 MPa are hidden. With this method, the number of hidden elements cannot be determined, but the investigation serves the qualitative comparison and shows from which backpressure force an improvement with respect to cracking or inhomogeneity can be expected in principle. Figure 7a shows the numerical investigations of *configuration A* without Johnson–Cook fracture criterion. Figure 7b shows the simulation with the determined Johnson–Cook parameters. When comparing the cross-section of the micrograph (Fig. 7c) with the result of the simulation of AA5083 after ECAP, similarities can be seen in the crack pattern of the specimen. The cracks are similarly deep and uniformly distributed on the sheet surface deformed by the inner channel

Fig. 6 (a) Equivalent plastic strain versus standardized sheet thickness for different mass scalings; (b) computing time for different mass scalings

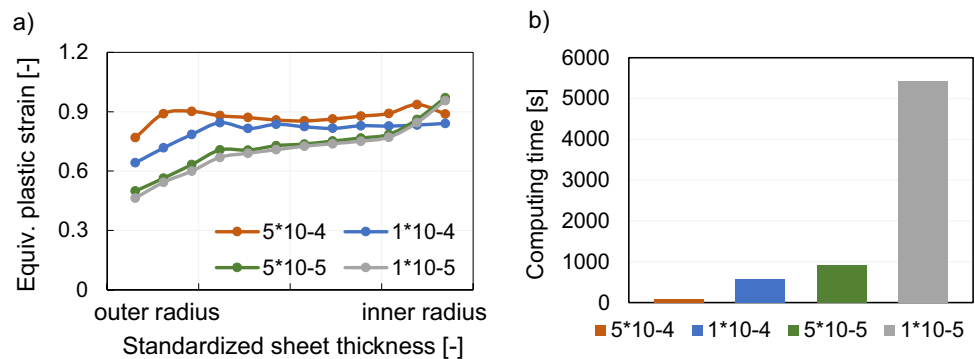
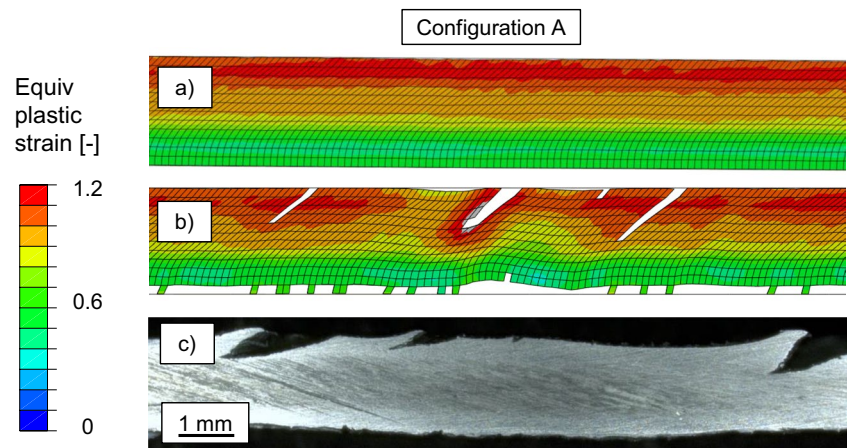


Fig. 7 Experimental and numerical results of the configuration A in comparison; (a) numerical results without Johnson–Cook criterion; (b) numerical results with Johnson–Cook criterion; (c) experimental results



radius. In the numerical study, it is clear that the cracking follows the course of the introduced shear, which is represented by the distortion of the elements. The numerical representation of these cracks demonstrates the suitability of the Johnson–Cook criterion determined in the push-out test for the use in ECAP simulations.

Experiments were also conducted for *configuration B* and Fig. 8 shows the comparison between the experimental and numerical cross-sections. Without the implementation of the Johnson–Cook fracture model, Fig. 8a shows a more uniform strain distribution than *configuration A*, but also decreasing especially towards the outer edge. By implementing the Johnson–Cook parameters, Fig. 8b shows inhomogeneities in the strain distribution at the outer radius. However, no obvious cracks compared to *configuration A* appear at the surface, which fits well with the experimental results from Fig. 5c.

The numerically determined equivalent plastic strain versus sheet thickness is shown in Fig. 9. The values were averaged along the ECAP direction in the length from 20 to 180 mm so that numerical boundary effects, e.g., at the heavily deformed leading edge of the sheet, are not included in the values. In addition, some values at the sheet surfaces (outer and inner radius on the x-axis) are omitted due to numerical discontinuities. The blue and gray curves show the numerical results of *configuration A*, the green and red curves *configuration B*. It can be seen that different strain values are obtained for modeling with and without the Johnson–Cook criterion. Although the curve remains similar, there are differences of up to 10%, especially on the outer side of the sheet. Since the qualitative comparison already showed that the simulation with fracture criterion corresponds well to the experiment, the curves with fracture criterion are interpreted below. *Configuration A* experiences a plastic strain of approx. 0.5 at the channel outer radius. The inner side shows strain peaks of up to 1.2. The strong inhomogeneity becomes clear from this curve progression. The strains in the channel *configuration B* are approx. 0.5

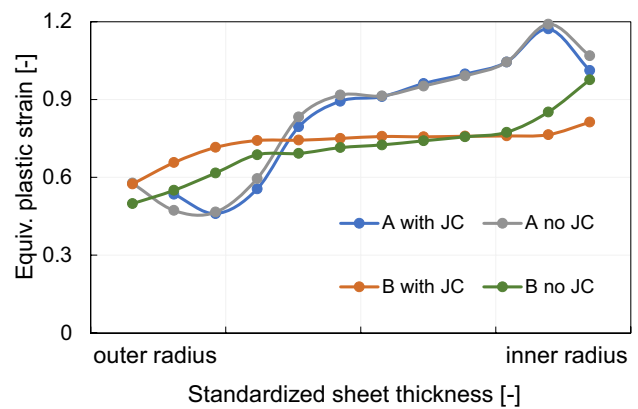


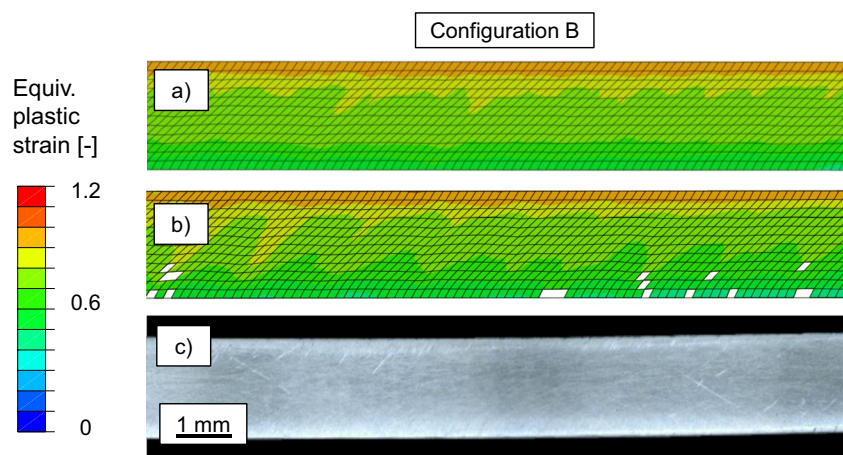
Fig. 9 Numerically determined equivalent plastic strain versus standardized sheet thickness from the outer corner radius up to the inner corner radius

on the outer side of the sheet and approx. 0.8 to 1 on the inner side. The strain distribution proves to be more homogeneous, particularly in the middle of the sheet. The results show that especially with the large ratio of the small sheet thickness to the sheet width, a small outer radius is essential to potentially suppress cracking and to promote a potential homogeneity of the microstructure. This behavior has already been shown for bulk material in conventional ECAP [35] and proves to be even more important in sheet metal ECAP due to scaling effects [36].

4 Integration and influence of backpressure in the sheet metal ECAP process

Many studies have already shown for ECAP with bulk material that backpressure has a positive influence on the homogeneity and the cracking of the material (sources). Especially with regard to an industrial use of the semi-finished

Fig. 8 Experimental and numerical results of the configuration B in comparison; (a) numerical results without Johnson–Cook criterion; (b) numerical results with Johnson–Cook criterion; (c) experimental results



product, these findings are very important. In the following investigations, the influence and amount of stress superposition by backpressure for sheet metal ECAP are discussed.

4.1 Numerical analysis of backpressure for sheet metal ECAP

In order to analyze the influence of backpressure (BP) on the aluminum sheet metal during the ECAP process, the numerical simulation was extended by additionally superimposing a uniform backpressure. For this purpose, 13 adjacent nodes were each subjected to the same force of 222 N, 667 N, and 1108 N, respectively. For the sheet cross-section of 288 mm², this resulted in a BP of 10 MPa, 30 MPa, or 50 MPa. Although this is lower than the BPs shown in previous studies (Figueiredo et al.: 80 MPa, Frint et al.: 200 MPa), Fig. 10 clearly indicates that, in the case of *configuration A*, cracks caused by the inner radius (Fig. 10a, without BP) are already avoided at the surface by a BP of 10 MPa (see Fig. 10b). At 30 MPa and 50 MPa, also both surfaces can be improved (see Fig. 10c). The material thus exhibits an intact surface even at low BPs in the numerical investigations, which makes further processing of the material possible as a result of the ECAP process.

If the plastic strains are compared over the sheet thickness, a slightly more homogeneous distribution is obtained for the backpressure of 30 MPa (see Fig. 11). Since the large outer radius of this configuration allows the material to be deflected and not sheared over the entire sheet thickness, a lower strain is obtained despite the backpressure in the outer area of the material. However, due to the superposition of the pressure and the resulting increased shear strain, the equivalent plastic strain increases towards the center of the

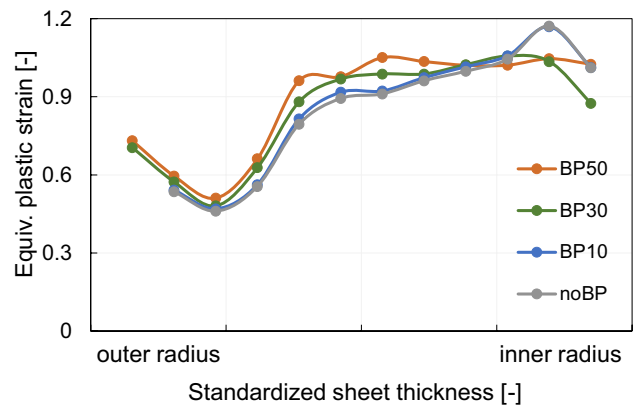


Fig. 11 Numerically determined equivalent plastic strain [-] versus standardized sheet thickness of configuration A with no backpressure, 10 MPa, 30 MPa, and 50 MPa

sheet and then remains at a constant value of approx. 1. The curve of the 50 MPa backpressure shows a similar behavior, but is on average slightly higher.

If the backpressure is applied to *configuration B*, the material is pressed into the outer radius (see Fig. 12). To represent the introduced stresses in the material, the von Mises equivalent stress is used. Figure 12a shows the stresses of the ECAP simulation of *configuration B* without BP; Fig. 12b shows the simulation with a BP of 10 MPa. The filling of the “dead zone” by the BP imposes a more uniform shear zone, which directly results in a more homogeneous and more deformed structure. This finding agrees well with the results of Ponce et al. (combination of inner and outer radius) and Filho et al. (focus on outer radius) who tested different channel geometries for bulk material [37, 38].

Fig. 10 ECAP simulation of configuration A (a) without backpressure, (b) with 10 MPa backpressure, (c) with 30 MPa backpressure, and (d) with 50 MPa backpressure

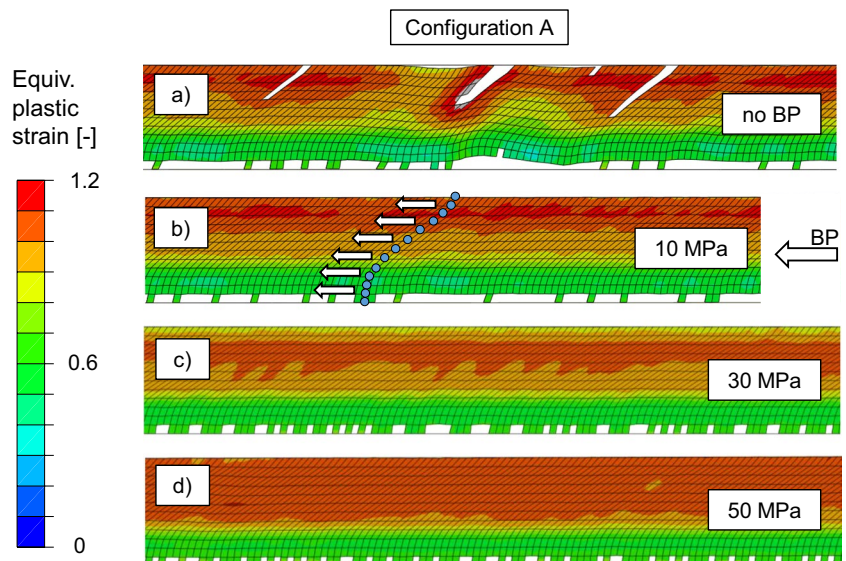


Fig. 12 ECAP simulation of configuration B (a) without backpressure and (b) with 10 MPa backpressure

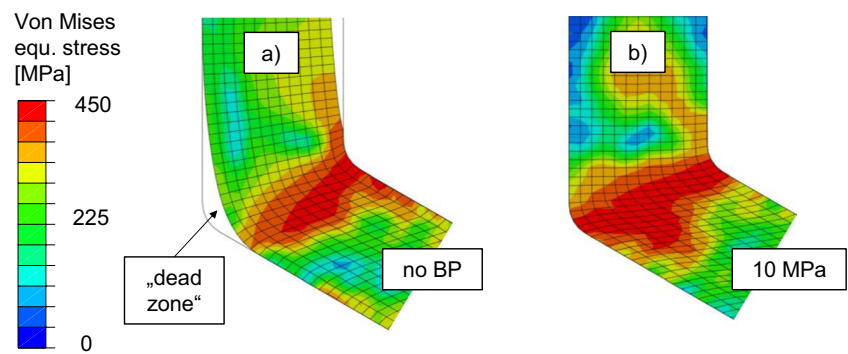


Fig. 13 ECAP simulation of configuration B (a) without backpressure, (b) with 10 MPa, (c) with 30 MPa, and (d) with 50 MPa backpressure

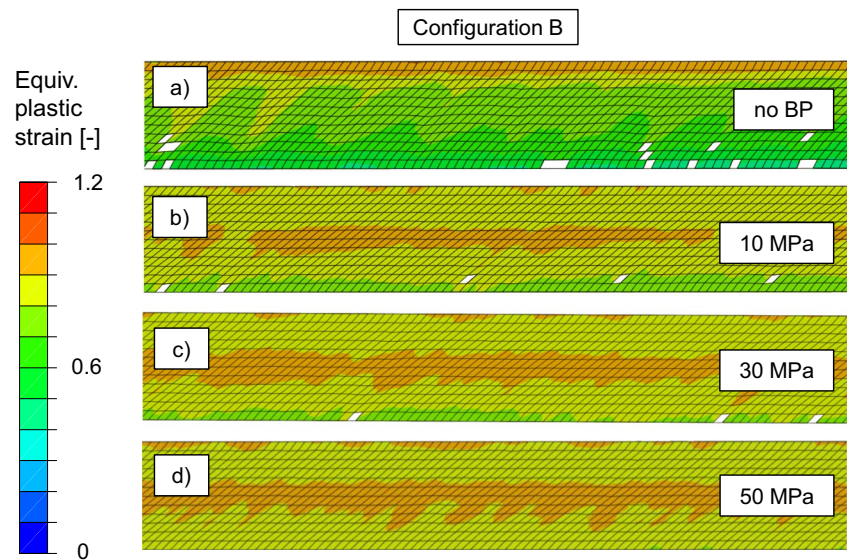


Figure 13 shows the distribution of plastic strains for configuration B. It is shown that the strains increase significantly at a BP of 10 MPa in the center of the sheet and a more homogeneous character develops (Fig. 13b). At 10 MPa, the strain values at the outer edge of the sheet are partially still low (approx. 0.6). At a BP of 30 MPa this inhomogeneity becomes smoother (see Fig. 10c). Also noticeable, with BP, are the locally increased strains reminiscent of shear bands [39]. However, to investigate these in detail, a more complex material model with kinematic hardening is needed [40]. This is beyond the scope of this paper but would be highly interesting for future research with respect to material engineering phenomena as shear band formation may also affect the local onset of surface failure.

Looking at the averaged strains over the sheet thickness, the advantages of the BP become apparent (see Fig. 14). The gray curve represents the ECAP process without backpressure. The solid blue line represents ECAP with a backpressure of 10 MPa. The result is a much more homogeneous strain profile in a range with strains from 0.8 to 0.9. If the backpressure is increased to 30 MPa, the strains

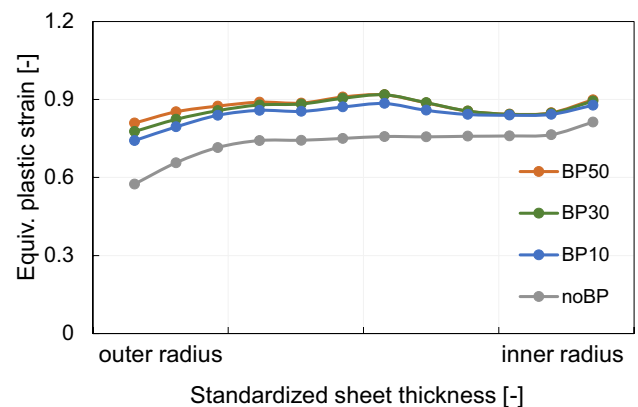


Fig. 14 Equivalent plastic strain [-] versus standardized sheet thickness of config. B with no backpressure, 10 MPa, 30 MPa, and 50 MPa

increase slightly. At the outer radius, the sheet is strongly pressed into the dead zone. In the simulation, this results in stress peaks at individual points, which is why the strain

values are much higher for 30 MPa and the sheet material already tends to break there.

The simulations of the backpressure show the potential for the improvement of the sheet metal ECAP. In particular, the simulations of the *configuration B* predict a homogeneous strain distribution due to the small outer radius and the closing of the “dead zone.” In the following, these numerical findings are used to develop a strategy for the implementation of the backpressure into the experiments with the *configuration B*.

4.2 Implementation of backpressure for sheet metal ECAP

Figure 15 shows the experimental implementation of BP in the ECAP tool for sheet materials. A backpressure device is developed and integrated into an additional base plate under the ECAP tool and positioned to the channel exit. The sheet is thus guided in a channel when BP is applied, in order to avoid buckling of the sheet. Furthermore, the counterpressure device was designed in such a way that only a small gap results between the channel exit of the angled die and the counterpressure device (see Fig. 15c). This also helps to avoid buckling. In Fig. 15b, it can be seen that the backpressure is applied via three gas springs. To apply a pressure of 10 MPa to the sheet, the three springs were filled with 19.2 bar nitrogen gas each (57.6 bar and 96 bar each for 30 MPa and 50 MPa). Due to the displacement of the pistons, the pressure in the springs increases, resulting in slight differences in backpressure at the beginning and end

of the ECAP process. The target values (10, 30, and 50 MPa) are therefore the pressures averaged over the process. After ECAP, the sheet metal is removed by opening eight screws and disassemble the upper counter channel. This would not be necessary in an industrialized variant, where it would be possible to move the upper channel part vertically with the right channel part (as with the previously existing tool) on the basis of the attachment to the downholder plate. Figure 15c shows the backpressure device in the closed state during the test. The experiments were performed for the *configuration B* and with the same parameters as ECAP without BP (punch speed: 6 mm/s; lubrication: Beruforge 152D) [41]. In order to introduce even higher and more homogeneous strains into the material, Route C was tested additionally. Therefore, the sheet material was turned 180° around ED after the first pass (N) and processed again.

4.3 Influence of backpressure on mechanical properties

In the following section, the ECAP-processed aluminum sheets with and without backpressure of *configuration B* are compared to the reference material. In order to characterize the homogeneity of the plastic deformation generated in the experiment, microhardness measurements are used. The microhardness of the ECAP sheets measured over the sheet thickness is shown in Fig. 16. For each of the experimental microhardness tests, three measurements were made across the sheet thickness, and the mean value is shown. Compared with the base hardness of 70.5 HV of

Fig. 15 (a) ECAP tool with the backpressure device; (b) backpressure device with the three gas springs; (c) picture of the ECAP tool for sheet metal with backpressure

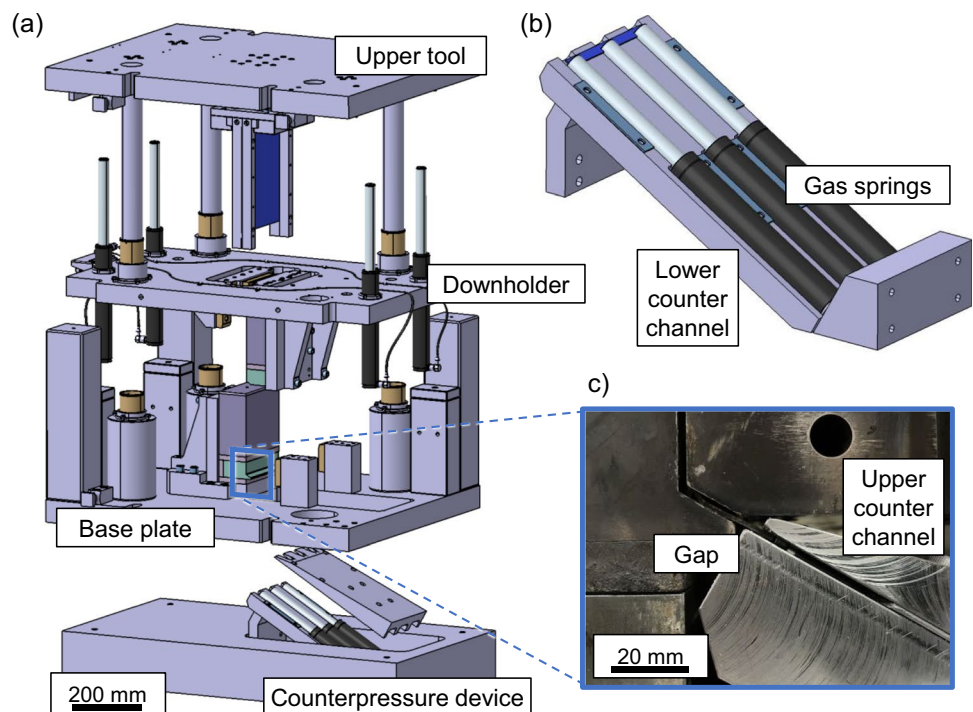
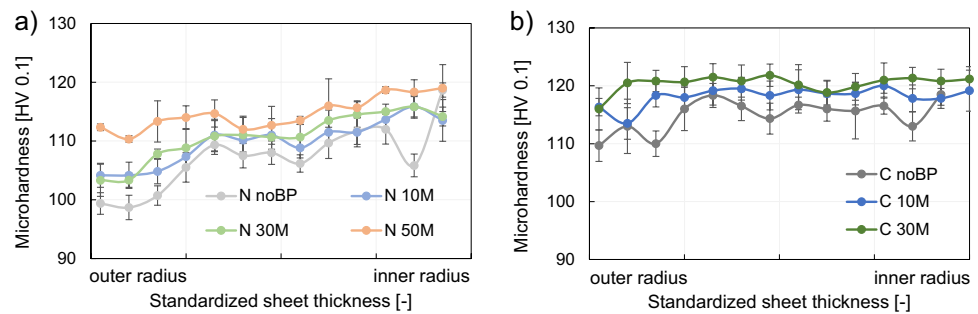


Fig. 16 Microhardness [HV0.1] versus standardized sheet thickness from the outer corner radius up to the inner corner radius

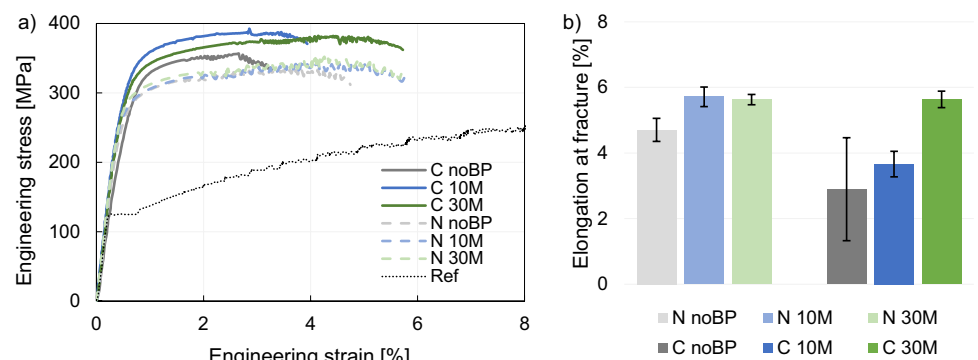


the initial material, an increase of hardness can be seen for the ECAP deformed material. For the first pass of ECAP (pass N, Fig. 16a) with no BP, a mean hardness of 107.2 ± 2 HV is found, wherein a hardness of ~ 100 HV is found in the outer area and a value of up to ~ 119 HV at the inner radius. The lower values at the outer radius correspond to the findings of the plastic strains in the simulation. In comparison, ECAP deformation with superimposed backpressure shows an overall increase in material hardness, accompanied by stabilization of microhardness at the inner channel radius (N 10 M: 109.8 ± 3.8 HV; N 30 M: 110.7 ± 4.1 HV; N 50 M: 114.6 ± 2.7 HV). For a backpressure of 50 MPa, the material starts to flow transversely due to the high backpressure and settles in the small gap between the channel outlet and the backpressure device, causing cracks on the surface. Since this gap was not considered in the simulation, this error could not be determined in the numerical analysis. For this reason, the sheets with 50 MPa could no longer be processed with more ECAP passes or tensile tests. Figure 16b illustrates the effects of backpressure in two ECAP passes. For Route C, the hardness values continue to increase, but without BP, strong fluctuations occur across the sheet thickness (C noBP: 114.9 ± 2.7 HV). For a BP of 10 MPa, a mean hardness of 118.2 ± 2.3 HV is determined and the fluctuations can already be reduced and with a BP of 30 MPa the distribution becomes even more homogeneous (C 30 M: 120.4 ± 2.6 HV). This homogeneity reflects the findings from the simulation and illustrates the potential of backpressure for ECAP of sheet materials.

In order to further investigate the macroscopic mechanical properties, tensile tests were carried out. Figure 17a shows the quasi-static engineering stress–strain curves for the non-processed reference material (Ref) and the ECAP states with and without BP at room temperature. Figure 17b summarizes the elongation to failure for the different setups. For every setup, three specimens of at least two different ECAP-processed sheets were tested. Representative data from individual specimens instead of mean values are shown in Fig. 17a, whereas Fig. 17b shows the mean values accompanied by standard deviations.

The base material shows a pronounced yield strength at 129 MPa and a distinctly serrated flow most likely due to the Portevin-Le Châtelier effect [11, 42]. The ultimate tensile strength is 290 MPa and the elongation to failure is approx. 21%, but just shown up to 8% in this diagram as the different ECAP setups are in the focus of this study. After the first ECAP pass (N), a distinct increase in the yield strength (YS) to a value of 256 MPa is observed without BP (+97%). The ultimate tensile strength (UTS) increases to 337 MPa without BP. In addition, the elongation to failure (EF) decreases to approx. 4.7%. For the first ECAP pass, a similar behavior can be found for the application of BP. For both backpressure values (10 and 30 MPa), YS increases to a value of approximately 280 MPa (+117%), while the UTS increases to 346 MPa for a BP of 10 MPa and to 344 MPa for a BP of 30 MPa, respectively. The reduction of EF is less pronounced with BP to 5.7% (10 MPa) and 5.6% (30 MPa) compared to the material deformed without BP. This suggests a

Fig. 17 (a) Engineering stress–strain curves from tensile testing of the initial (gray) and ECAP-processed sheet metals at room temperature under quasi-static loading and (b) elongation at fracture



more homogeneous distribution and a better surface of the BP samples and also agrees with the microhardness results discussed above. However, there is a greater difference in the results of route C. Without BP, route C results in a YS of 278 MPa (+115%). For the BP setups, these YS values increase to 335 MPa (BP 10 MPa, +157%) and 325 (BP 30 MPa, +150%), respectively. In the maximum elongation, without BP, the mean value is 2.9% with scatter of 1.5%. The values are with BP at 3.7% (BP 10 MPa) and 5.6% (BP 30 MPa) and thus significantly higher. Especially the scattering of 0.4% and 0.3% shows the advantages of the BP in the case of sheet metal ECAP. Both the increase in yield strength and the decrease in elongation compared to the reference material can be attributed to microstructural defects. This is consistent with the findings of the ECAP process for AA5083 bulk material [43, 44]. Especially with regard to the strongly decreasing elongation, it also becomes apparent that due to the significantly changed ratio of thickness to sheet width, edge effects have a greater influence on the properties of the material [45]. It is therefore important to prevent these edge effects by skillful process control and it is shown that BP can be a beneficial contribution with respect to these effects.

4.4 Microstructural analysis

Qualitatively, the characteristic changes in terms of mechanical properties during ECAP can also be related to microstructural evolution by considering the results of scanning electron microscopy (SEM), particularly electron backscatter diffraction (EBSD), performed on the microstructure of the sheet cross-sections. This kind of analysis is briefly discussed below.

Samples for microstructural investigations were subjected to a conventional mechanical grinding and polishing procedure followed by colloidal silica polishing. The microstructural features of all states were examined in the transverse direction (TD) of the sheets. The EBSD measurements were performed using a Zeiss Neon 40 EsB field-emission scanning electron microscope equipped with a DigiView IV EBSD camera (EDAX Inc., Mahwah, NJ, USA), applying an acceleration voltage of 15 kV and a step size of 1 μm . EBSD raw data were postprocessed by a slight clean-up including a confidence index neighbor correlation and grain dilation. Grains were defined as having a minimum grain size of 3 in the OIM analysis software (ver. 6). For the characterization of substructures, as well as grains with high-angle grain boundaries, grain tolerance angles of 5° (TA-5°) and 15° (TA-15°) were used, respectively. The microstructures of the sheet material for the reference condition (Ref) as well as the ECAP-processed materials after two accumulative ECAP passes in *configuration B* are shown in Fig. 18. The black lines in the orientation

maps (Fig. 18a–c) represent high-angle grain boundaries (misorientation angles > 15°). Figure 18a shows a representative EBSD micrograph of the cross-section for the initial condition (Ref). The microstructure is characterized by homogeneously distributed, equiaxed grains. The corresponding grain size distribution (black) in Fig. 18d shows a distinct peak at about 16 μm for TA-5°, while a slightly higher mean grain size of 20 μm is observed for TA-15° (Fig. 18e). The material deformed in two accumulative ECAP passes without backpressure (C noBP) shows a pronounced deformation gradient from the upper to the lower sheet edge. At the upper edge of the sheet, a narrow region can be seen where the material is sheared in the opposite direction to the pressing direction. This is most likely due to the large friction in the surface area. This section is followed by a region in which the longitudinal semi-axes of the grains are aligned at a certain characteristic tilt angle with respect to the extrusion direction (ED) due to the shear strains. The lower third of the sheet cross-section, on the other hand, shows no signs of pronounced deformation. In the TA-15° grain size distribution (Fig. 18e), this is evident from a flattened peak between 15 and 28 μm (gray). The TA-5° distribution (Fig. 18d), on the other hand, shows a slight shift of the peak related to substructures to smaller sizes. A significant change in microstructure can be seen in Fig. 18c for the condition deformed in two accumulative ECAP passes with a backpressure of 10 MPa (C 10 M). The microstructure is characterized by gradients similar to those already described for the C state without BP. The grains of the lower third of the sheet cross-section now also appear to be oriented at a certain characteristic angle of inclination with respect to ED and a slightly higher number of high-angle grain boundaries as well as pronounced substructures can be observed. It should be noted that Fig. 18c) is shown at a slightly different magnification to allow the entire sheet cross-section to be imaged with its characteristic features (including deformation gradients, grain orientations, and local substructures). The TA-15° distribution (Fig. 18e) shows a minor increase in the range of smaller grain sizes at about 4 μm . In contrast, the TA-5° distribution of substructures (Fig. 18d) shows a significant increase for structures below a size of 8 μm . The trend of a significant increase in defect density as a result of the ECAP deformation, as well as the further increase due to the application of a passive backpressure, is further illustrated by the boundary line length per area (interfacial density as a function of misorientation angle) in Fig. 18f. This plot shows a significant increase of all boundaries for the ECAP conditions (C noBP, C 10 M) compared to the reference material (Ref). The application of a backpressure of 10 MPa (C 10 M) then leads to a further increase, especially for boundaries with misorientations of more than 10°. The microstructural results clearly show that the increase in mechanical strength

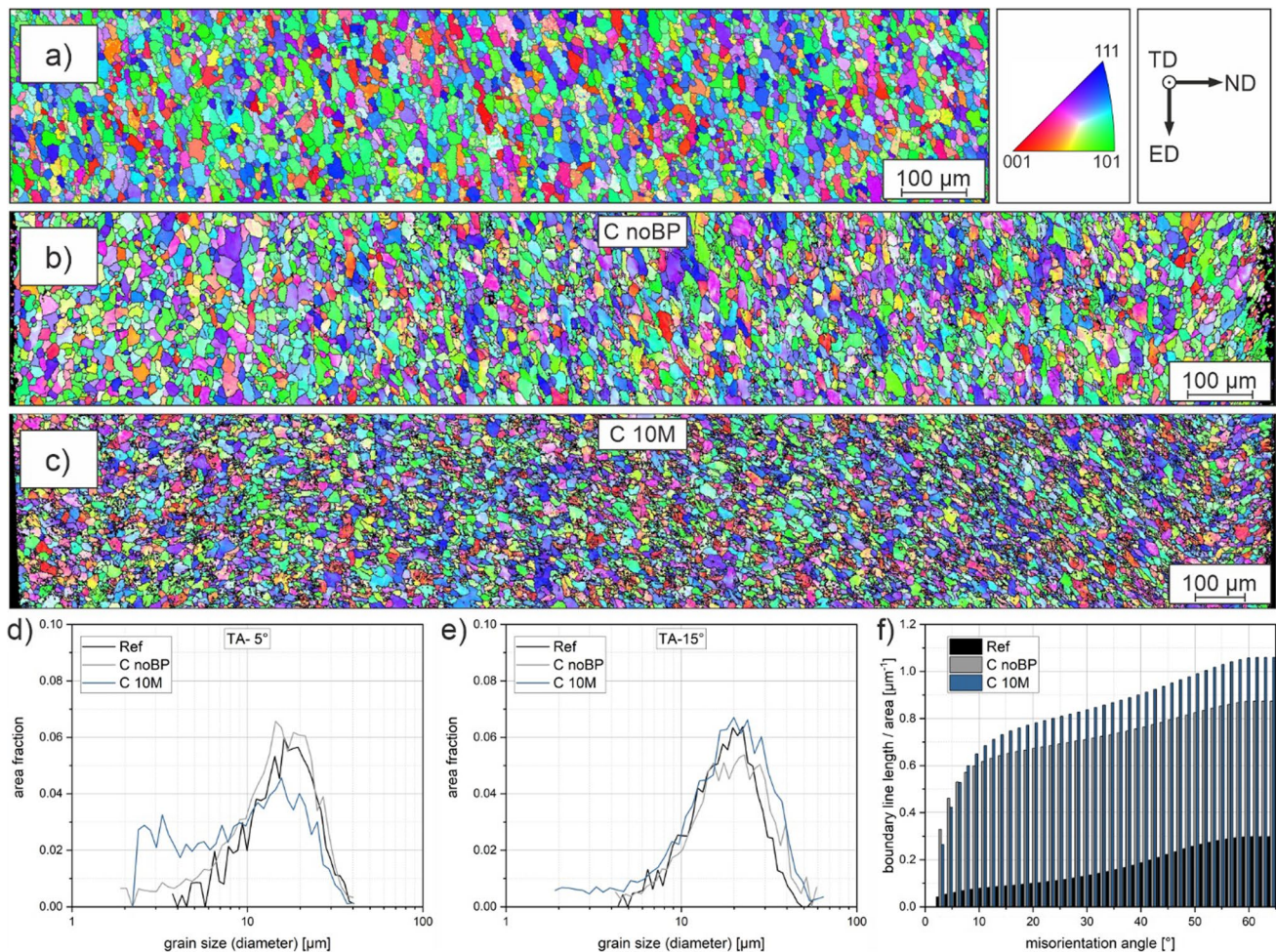


Fig. 18 Orientation maps of the microstructures of the sheet metals cross-section (TD plane): (a) reference material (Ref), configuration B, and route C (b) without (C noBP) and (c) with an amount of 10 MPa backpressure (C 10 M); corresponding grain size distribu-

tions for a grain tolerance angle of (d) 5° (TA-5°) and (e) 15° (TA-15°); (f) quantitative analysis of the boundary density as a function of the misorientation angle

is based on the formation of new defect boundaries. The additional substructures with low-angle as well as new high-angle grain boundaries are effective obstacles for dislocation motions during further deformation, resulting in the macroscopically increased strength [4].

5 Summary and conclusions

In the present study, a modification of the ECAP process for aluminum sheet metal AA5083 was investigated. Based on preliminary experimental investigations, numerical models were built and validated. With the validated models, appropriate adjustments to the novel manufacturing technique for sheet metal were made and systematically investigated. The main findings are summarized in the following key points:

- The Johnson–Cook fracture criterion can be calibrated for numerical investigations using the push-out test. A possible surface cracking in experiments can thus be reproduced in ECAP simulations.
- Both the simulations and the experimentally performed deformations show that even small amounts of backpressure (10 MPa) result in a sufficient suppression of crack formation and a more homogeneous distribution of the applied strains in the ECAP for sheet materials. With backpressure, ECAP route C can be performed successfully for aluminum AA5083 sheet materials.
- The experimental investigations show the potential of sheet metal ECAP. Mechanical properties similar to those obtained in previous studies with bulk material were obtained (yield strength + 157%). EBSD measurements show a significant increase in substructures, explaining the macromechanical findings.

The microhardness results and mechanical properties show the deformation stored the sheet material by the ECAP process. To further improve the strain behavior, it is recommended to use targeted post and intermediate heat treatments in follow-up investigations. With a combination of heat treatment and multiple ECAP passes, it is possible to use the results to specifically integrate the ECAP process into the semi-finished product production to create a further advantage in the use and energy efficiency of aluminum alloys. In addition, the studies offer the potential to investigate the effects of scaling in even greater detail by using different sheet thicknesses for the studies.

Acknowledgements Thank you to Maria Schmuck who helped to perform the microhardness tests. The authors also acknowledge Thomas Spoerer who contributed to the installation of the backpressure tool and Yiheng Yang who contributed to the simulations in their student research projects.

Author contribution Maximilian Gruber: conceptualization, methodology, investigation, software, writing—original draft, writing—review and editing, visualization, formal analysis, data curation. Christian Illgen: conceptualization, methodology, investigation, formal analysis, validation. Felix Lichte: investigation, validation. Christoph Hartmann: investigation, conceptualization, validation. Philipp Frint: investigation, conceptualization, project administration, validation. Martin F.-X. Wagner: supervision, project administration, validation, funding acquisition. Wolfram Volk: supervision, project administration, validation, funding acquisition.

Funding Open Access funding enabled and organized by Projekt DEAL. The authors gratefully acknowledge the German Research Foundation (Deutsche Forschungsgemeinschaft, DFG) for supporting this work carried out within the framework of the collaborative research project with the grant numbers 376797652 (VO 1487/32–1 and WA 2602/13–1).

Data availability The data that support the findings of this study are available from the corresponding author upon reasonable request. Source data are provided with this paper.

Code availability Not applicable.

Declarations

Ethics approval Not applicable.

Consent to participate Not applicable.

Consent of publication All authors have consented to the submission of this article to the journal.

Conflict of interest The authors declare no competing interests.

Open Access This article is licensed under a Creative Commons Attribution 4.0 International License, which permits use, sharing, adaptation, distribution and reproduction in any medium or format, as long as you give appropriate credit to the original author(s) and the source, provide a link to the Creative Commons licence, and indicate if changes were made. The images or other third party material in this article are

included in the article's Creative Commons licence, unless indicated otherwise in a credit line to the material. If material is not included in the article's Creative Commons licence and your intended use is not permitted by statutory regulation or exceeds the permitted use, you will need to obtain permission directly from the copyright holder. To view a copy of this licence, visit <http://creativecommons.org/licenses/by/4.0/>.

References

1. Jaeger H, Gude M (2019) Lightweight materials in tomorrow's automotive industry. *Lightweight Design worldwide*:20–23
2. Azushima A, Kopp R, Korhonen A, Yang DY, Micari F, Lahoti GD, Groche P, Yanagimoto J, Tsuji N, Rosochowski A, Yanagida A (2008) Severe plastic deformation (SPD) processes for metals. *CIRP Ann* 57:716–735. <https://doi.org/10.1016/j.cirp.2008.09.005>
3. Langdon TG (2010) Processing by severe plastic deformation: historical developments and current impact. *MSF* 667–669:9–14. <https://doi.org/10.4028/www.scientific.net/MSF.667-669.9>
4. Valiev RZ, Islamgaliev RK, Alexandrov IV (2000) Bulk nanostructured materials from severe plastic deformation. *Prog Mater Sci* 45:103–189
5. Hellmig RJ (2008) Hochgradige plastische Umformung durch Equal Channel Angular Pressing (ECAP). Technische Universität Clausthal, Habilitation
6. Lowe TC, Zhu YT (2003) Commercialization of nanostructured metals produced by severe plastic deformation processing. *Adv Eng Mater* 5:373–378. <https://doi.org/10.1002/adem.200310076>
7. Iwahashi Y, Wang J, Horita Z, Nemoto M, Langdon TG (1996) Principle of equal-channel angular pressing for the processing of ultra-fine grained materials. *Scripta Mater* 35:143–146
8. Sklenička V, Král P, Ilucová L, Saxl I, Dvořák J, Svoboda M (2006) Inhomogeneity of microstructure and creep of ECAP aluminium. *MSF* 503–504:245–250. <https://doi.org/10.4028/www.scientific.net/MSF.503-504.245>
9. Frint P, Wagner MF-X (2019) Strain partitioning by recurrent shear localization during equal-channel angular pressing of an AA6060 aluminum alloy. *Acta Mater* 176:306–317. <https://doi.org/10.1016/j.actamat.2019.07.009>
10. Semiatin SL, DeLo DP, Shell EB (2000) The effect of material properties and tooling design on deformation and fracture during equal channel angular extrusion. *Acta Mater* 48:1841–1851. [https://doi.org/10.1016/S1359-6454\(00\)00019-7](https://doi.org/10.1016/S1359-6454(00)00019-7)
11. Fritsch S, Scholze M, Wagner MF-X (2012) Cryogenic forming of AA7075 by Equal-Channel Angular Pressing. *Mat-wiss u Werkstofftech* 7:561–566. <https://doi.org/10.1002/mawe.201200001>
12. Segal VM, Reznikov VI, Drobyshevskiy AE, Kopylov VI (1981) Plastic working of metals by simple shear. (english translation). *Russ Metall* 1:115–123
13. Lapovok R (2005) The role of back-pressure in equal channel angular extrusion. *J Mater Sci* 40:341–346
14. Figueiredo RB, Cetlin PR, Langdon TG (2010) Stable and unstable flow in materials processed by equal-channel angular pressing with an emphasis on magnesium alloys. *Metall and Mat Trans A* 41:778–786. <https://doi.org/10.1007/s11661-009-0100-2>
15. Frint P, Hockauf M, Halle T, Wagner M-X, Lampke T (2012) The role of backpressure during large scale Equal-Channel Angular Pressing. *Mat-wiss u Werkstofftech* 43:668–672. <https://doi.org/10.1002/mawe.201200015>
16. Stolyarov V, Lapovok R, Brodova I, Thomson P (2003) Ultrafine-grained Al–5 wt.% Fe alloy processed by ECAP with

- backpressure. *Mater Sci Eng, A* 357:159–167. [https://doi.org/10.1016/S0921-5093\(03\)00215-6](https://doi.org/10.1016/S0921-5093(03)00215-6)
17. Iwahashi Y, Horita Z, Nemoto M, Langdon TG (1997) An investigation of microstructural evolution during Equal-Channel Angular Pressing. *Acta Mater* 45:4733–4741
 18. Cetlin PR, Aguilar MTP, Figueiredo RB, Langdon TG (2010) Avoiding cracks and inhomogeneities in billets processed by ECAP. *J Mater Sci* 45:4561–4570. <https://doi.org/10.1007/s10853-010-4384-9>
 19. Illgen C, Frint P, Gruber M, Volk W, Wagner MF-X (2020) Evolution of grain refinement in AA5083 sheet metal processed by ECAP. DOI: 10.1007/978-3-030-36408-3_52. In: Tomsett A (ed) *Light Metals 2020*. Springer International Publishing, Cham, pp 362–369
 20. Gruber M, Illgen C, Frint P, Wagner MF-X, Volk W (2019) Numerical and experimental study on ECAP-processing parameters for efficient grain refinement of AA5083 sheet metal. *KEM* 794:315–323. <https://doi.org/10.4028/www.scientific.net/KEM.794.315>
 21. DIN 50125 (2004) Prüfung metallischer Werkstoffe – Zugproben(50125)
 22. DIN EN ISO 6892–1 (2014) Metallische Werkstoffe – Zugversuch – Teil 1: Prüfverfahren bei Raumtemperatur(6892–1)
 23. DIN EN ISO 16808 (2014) Metallische Werkstoffe – Blech und Band – Bestimmung der biaxialen Spannung/Dehnung-Kurve durch einen hydraulischen Tiefungsversuch mit optischen Messsystemen(16808)
 24. Gosh AK (1977) Tensile instability and necking in materials with strain hardening and strain-rate hardening. *Acta Metall* 25:1413–1424
 25. Hockett JE, Sherby OD (1975) Large strain deformation of polycrystalline metals at low homologous temperatures. *J Mech Phys Solids* 23:87–98
 26. Alkorta J, Gil Sevillano J (2003) A comparison of FEM and upper-bound type analysis of equal-channel angular pressing (ECAP). *J Mater Process Technol* 141:313–318. [https://doi.org/10.1016/S0924-0136\(03\)00282-6](https://doi.org/10.1016/S0924-0136(03)00282-6)
 27. Figueiredo RB, Pinheiro IP, Aguilar MTP, Modenesi PJ, Cetlin PR (2006) The finite element analysis of equal channel angular pressing (ECAP) considering the strain path dependence of the work hardening of metals. *J Mater Process Technol* 180:30–36. <https://doi.org/10.1016/j.jmatprotec.2006.04.017>
 28. El-Shenawy M, Ahmed MMZ, Nassef A, El-Hadek M, Alzahrani B, Zedan Y, El-Garaihy WH (2021) Effect of ECAP on the plastic strain homogeneity, microstructural evolution, crystallographic texture and mechanical properties of AA2xxx aluminum alloy. *Metals* 11:938. <https://doi.org/10.3390/met11060938>
 29. Greß T, Stahl J, Mittler T, Spano L, Chen H, Ben Khalifa N, Volk W (2019) Mechanical characterization of as-cast AA7075/6060 and CuSn6/Cu99.5 compounds using an experimental and numerical push-out test. *Mater Sci Eng, A* 751:214–225. <https://doi.org/10.1016/j.msea.2019.02.080>
 30. Johnson GR, Cook WH (1985) Fracture characteristics of three metals subjected to various strains strainrates temperatures and pressures. *Eng Fract Mech* 21:31–48
 31. Zhang C, Leotoing L, Guines D, Ragneau E (2009) Theoretical and numerical study of strain rate influence on AA5083 formability. *J Mater Process Technol* 209:3849–3858. <https://doi.org/10.1016/j.jmatprotec.2008.09.003>
 32. VDI 2906–2 (1994) Schnittflächenqualität beim Schneiden, Beschneiden und Lochen von Werkstücken aus Metall
 33. Greß T, Gruber M, Stahl J, Wittmann S, Steinlehner F, GlückNardi V, Tonn B, Volk W (2020) Experimental and numerical investigations into the deformation and fracture behavior of intermetallics and base materials in as-cast Al-Cu compounds. *Mater Today Commun* 25:101278. <https://doi.org/10.1016/j.mtcomm.2020.101278>
 34. Gruber M, Yang Y, Illgen C, Frint P, Wagner MF-X, Volk W (2021) Thermomechanical analysis and experimental validation of ECAP for aluminum sheet metal. 10.1007/978-3-030-75381-8_149. In: Daehn G, Cao J, Kinsey B et al (eds) *Forming the Future*, vol 1. Springer International Publishing, Cham, pp 1775–1790
 35. Skrotzki W (2019) Deformation heterogeneities in equal channel angular pressing. *Mater Trans* 60:1331–1343. <https://doi.org/10.2320/matertrans.MF201926>
 36. Vollertsen F, Biermann D, Hansen HN, Jawahir IS, Kuzman K (2009) Size effects in manufacturing of metallic components. *CIRP Ann* 58:566–587. <https://doi.org/10.1016/j.cirp.2009.09.002>
 37. A Mendes Filho AA de, Sordi VL, Rubert JB, Ferrante M (2008) The influence of ECAP die channel geometry on shear strain and deformation uniformity. *MSF* 584-586:145–150. <https://doi.org/10.4028/www.scientific.net/MSF.584-586.145>
 38. Ponce-Peña P, López-Chipres E, García-Sánchez E, Escobedo-Bretado MA, Ochoa-Salazar BX, González-Lozano MA (2015) Optimized design of an ECAP die using the finite element method for obtaining nanostructured materials. *Advances in Materials Science and Engineering*:1–8. <https://doi.org/10.1155/2015/702548>
 39. Figueiredo RB, Aguilar MTP, Cetlin PR (2006) Finite element modelling of plastic instability during ECAP processing of flow-softening materials. *Mater Sci Eng, A* 430:179–184. <https://doi.org/10.1016/j.msea.2006.05.116>
 40. Horn T, Silbermann C, Frint P, Wagner M, Ihlemann J (2018) Strain localization during equal-channel angular pressing analyzed by finite element simulations. *Metals* 8:55. <https://doi.org/10.3390/met8010055>
 41. Gruber M, Leitner P, Auer M, Illgen C, Frint P, Wagner MF, Volk W (2022) A novel method for the determination of high temperature FLCs of ECAP-processed aluminum AA5083 sheet metal. *KEM* 926:1039–1050. <https://doi.org/10.4028/p-w5x675>
 42. Joshi SP, Eberl C, Cao B, Ramesh KT, Hemker KJ (2009) On the occurrence of Portevin–Le Châtelier instabilities in ultrafine-grained 5083 aluminum alloys. *Exp Mech* 49:207–218. <https://doi.org/10.1007/s11340-008-9208-3>
 43. Chang S-Y, Lee JG, Park K-T, Shin DH (2001) Microstructures and mechanical properties of ECAP 5083 Al Alloy. *Mater Trans* 42:1074–1080
 44. Baig M, Rehman AU, Mohammed JA, Seikh AH (2021) Effect of microstructure and mechanical properties of Al5083 alloy processed by ECAP at room temperature and high temperature. *Crystals* 11:683. <https://doi.org/10.3390/cryst11060683>
 45. Horita Z, Fujinami T, Langdon TG (2001) The potential for scaling ECAP: effect of sample size on grain refinement and mechanical properties. *Mater Sci Eng, A* 318:34–41

Publisher's note Springer Nature remains neutral with regard to jurisdictional claims in published maps and institutional affiliations.